

Superconducting phase transitions in disordered NbTiN films

M. V. Burdastyh^{1,2}, S. V. Postolova^{1,3}, T. Proslie⁴, S. S. Ustavshikov³, A. V. Antonov³, V. M. Vinokur⁵, and A. Yu. Mironov^{1,2}

¹A. V. Rzhhanov Institute of Semiconductor Physics SB RAS, 13 Lavrentjev Avenue, Novosibirsk 630090, Russia

²Novosibirsk State University, Pirogova str. 2, Novosibirsk 630090, Russia

³Institute for Physics of Microstructures RAS, GSP-105, Nizhny Novgorod 603950, Russia

⁴Institut de recherches sur les lois fondamentales de l'univers, Commissariat de l'énergie atomique et aux énergies renouvelables-Saclay, Gif-sur-Yvette, France

⁵Materials Science Division, Argonne National Laboratory, 9700 S. Cass Ave, Argonne, IL 60439, USA

ABSTRACT

The suppression of superconductivity in disordered systems is a fundamental problem of condensed matter physics. Here we investigate the superconducting niobium-titanium-nitride ($\text{Nb}_{1-x}\text{Ti}_x\text{N}$) thin films grown by atomic layer deposition (ALD) where disorder is controlled by the slight tuning of the ALD process parameters. We observe the smooth crossover from the disorder-driven superconductor-normal metal transition (often referred to as fermionic mechanism) to the case where bosonic mechanism dominates and increasing disorder leads to formation of metal with Cooper pairing. We show that, in 'moderately' disordered films, the transition to zero-resistance state occurs in a full agreement with the conventional theories of superconducting fluctuations and Berezinskii-Kosterlitz-Thouless transition. However, the 'critically' disordered films violate this accord showing low-temperature features possibly indicating the Bose metal phase. We show that it is the interrelation between film's sheet resistance in the maximum, R_{\max} , of the resistive curve $R_{\square}(T)$ and $R_{\text{q}} = h/4e^2$ that distinguishes between these two behaviors. We reveal the characteristic features in magnetoresistance of the 'critically' disordered films with $R_{\max} > R_{\text{q}}$.

Introduction

The superconductor-insulator transitions (SIT) observed in a wealth of various systems (^{1,2}), are usually divided in two different categories depending on the assumed mechanism of superconductivity suppression — fermionic³ or bosonic^{4,5}. The fermionic scenario proposes that disorder destroys the Cooper pairs. In this case, as the normal state sheet resistance $R_{\square\text{N}}$ increases, both superconducting critical temperature T_{c} (where the life-time of fluctuating Cooper pairs diverges) and $T_{\text{BK}}T$ temperature (where the global phase coherence establishes in a system) decrease down to zero and then the superconductor-metal transition occurs due to the complete disappearance of the Cooper pairs, and the suppression of T_{c} with $R_{\square\text{N}}$ is described by Finkel'stein formula³. Such a behaviour is observed, for example, in thin films of niobium nitride NbN ^{6,7}. Within the bosonic scenario, increasing disorder localizes Cooper pairs, which exist in the insulating state. Hence, as $R_{\square\text{N}}$ increases, T_{c} decreases weakly and $T_{\text{BK}}T$ decreases down to zero. In this scenario the SIT occurs through a single point of the metal phase with the critical sheet resistance $R_{\text{q}} = h/4e^2 = 6.45 \text{ k}\Omega$ ⁵. Experimentally, the critical sheet resistance is not universal and varies in the range between approximately $R_{\text{q}}/2$ and $3R_{\text{q}}$. The direct disorder-driven SIT is observed, for example, in indium oxide InO_x ⁸⁻¹⁰ and titanium nitride TiN ^{11,12} films. At present, the interrelation between these mechanisms as well as the nature of the possible intermediate Bose metal¹³⁻¹⁶ still are not completely understood and are intensively debated^{2,17}.

Here we examine the approach to the disorder-driven SIT in a few sets of $\text{Nb}_{1-x}\text{Ti}_x\text{N}$ films grown by ALD technique. The difference between sets is in the slight shift of ALD parameters: the fraction x and the temperature of deposition T_{ALD} . We show that with x increasing and T_{ALD} decreasing the smooth crossover occurs from fermionic mechanism of superconductivity suppression to the case when both bosonic and fermionic mechanisms are involved. We show that superconducting NbTiN films fall into two categories depending on a ratio between R_{q} and R_{\max} , the sheet resistance in the maximum of the $R_{\square}(T)$ curve. We reveal the intrinsic difference between films with R_{\max}/R_{q} smaller and greater than unity through quantitatively distinct behaviours of the magnetoresistance.

Samples preparation and characterization

To grow suitable NbTiN films, we employ the atomic layer deposition (ALD) technique based on sequential surface reaction step-by-step film growth. This highly controllable process provides superior thickness and stoichiometric uniformity and an atomically smooth surface^{18,19} as compared to chemical vapor deposition, the standard technique

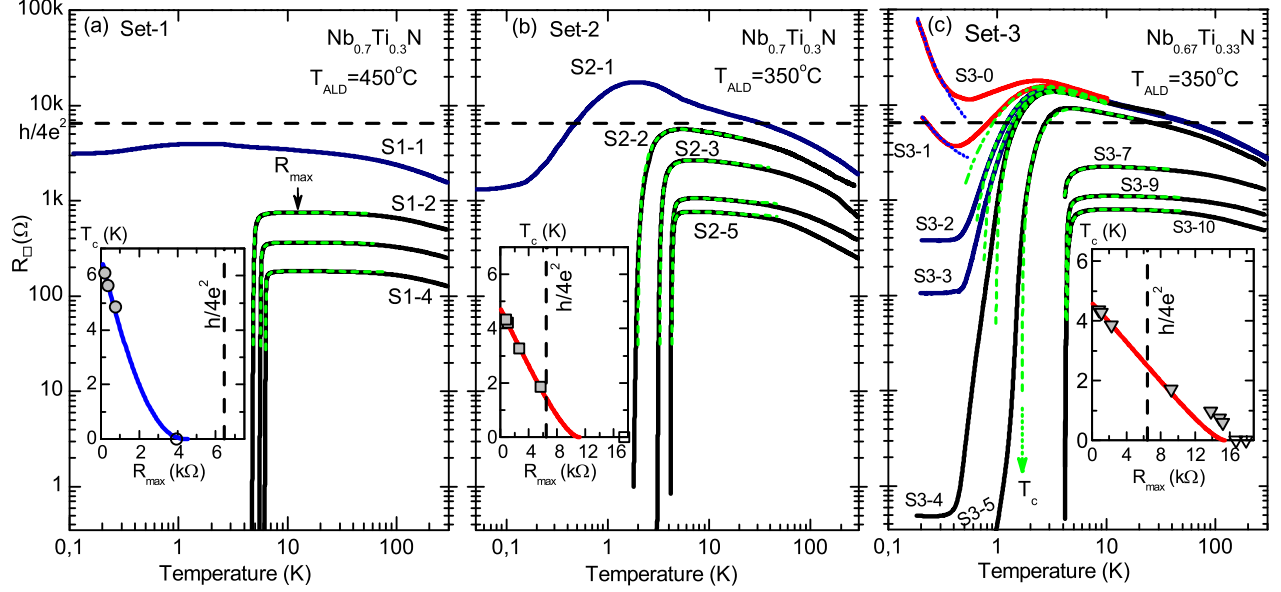


Figure 1. Sheet resistance R_{\square} vs. temperature on log-log scale for films of Set-1 (a), Set-2 (b) and Set-3 (c). The deposition temperature T_{ALD} and Ti fraction x in $\text{Nb}_{1-x}\text{Ti}_x\text{N}$ composition are given on the plots (see SI for the line-log scale). The vertical axis scale is same for all plots. Solid lines are experimental dependencies. Horizontal line shows the resistance $R_q = h/4e^2 = 6.45 \text{ k}\Omega$. Dashed line: fits accounting for contributions to conductance from superconducting fluctuations (SF), the T_c obtained from these fits are given in Table. (c) Dotted line: activation dependence $R_{\square} \propto \exp(1/T)$. Sample S3-5 doesn't manifest BKT transition (see Fig. 2 (b), (d)). Insets: T_c vs. sheet resistance in maximum R_{max} prior to superconducting resistance drop, symbols are the experimental values, the solid line is the theoretical fitting by Eq. (1) with the adjustable parameter $\gamma = 6.5$ ($T_{c0} = 6.71 \text{ K}$) for (a); $\gamma = 4.4$ ($T_{c0} = 4.75 \text{ K}$) for (b); and $\gamma = 3.8$ ($T_{c0} = 4.6 \text{ K}$) for (c). Vertical line shows the R_q . Open symbols with $T_c = 0$ correspond to samples for which we can not reliably define T_c with SF-fits.

used to grow NbTiN films²⁰. We used NbCl_5 , TiCl_4 , and NH_3 as gaseous reactants; the stoichiometry was tuned by varying the ratio of $\text{TiCl}_4/\text{NbCl}_5$ cycles during growth²¹. The superconducting properties of these ultrathin NbTiN films were optimized by utilizing AlN buffer layers grown on top of the Si substrate²². All films have a fine-dispersed polycrystalline structure²³ with the average crystallite size being $\approx 5 \text{ nm}$.

Three sets of $\text{Nb}_{1-x}\text{Ti}_x\text{N}$ films are grown varying deposition temperature T_{ALD} and fraction of Ti x . For Set-1 $T_{\text{ALD}} = 450^\circ\text{C}$, and $T_{\text{ALD}} = 350^\circ\text{C}$ for Set-2 and Set-3. The Ti fraction $x = 0.3$ in Set-1 and Set-2 and $x = 0.33$ in Set-3. Films within single Set are grown varying the number of ALD cycles, that provides films of different thickness d . The parameters of samples are given in the Table. The Hall carrier density n (see SI) appears to be approximately the same regardless of the disorder $n \sim 10^{22} \text{ cm}^{-3}$ which is one order smaller than in NbTiN films examined in²⁴.

Results and discussion

Figure 1 presents the temperature dependencies of the sheet resistance R_{\square} for three our Sets of films. Before going into details, we'd like to highlight a qualitative difference between Set-1 and Sets-2,3. The superconductivity in Set-1 (Fig. 1(a)) gets fully suppressed by disorder before the sheet resistance of samples in maximum R_{max} reaches critical value $R_q = h/4e^2 = 6.45 \text{ k}\Omega$. In Set-3 (and most likely in Set-2), samples with $R_{\text{max}} > R_q$ still experience superconducting transition, and Sets-2,3 demonstrate more complicated evolution.

In all samples the resistances first grow with cooling down from room temperature (see Fig.3 in SI for the discussion of high-temperature behaviour of $R_{\square}(T)$). With further cooling, the $R_{\square}(T)$ dependencies first reach maximum R_{max} and after that behave differently in different Sets.

The transition into a superconducting state is a two-stage process in thin films: first, the finite amplitude of the order parameter forms at the superconducting critical temperature T_c , second, a global phase-coherent state establishes at lower temperature T_{BKT} of the Berezinskii-Kosterlitz-Thouless transition. Below we analyze suppression of both these temperatures with disorder.

Taking into account perturbative quantum contributions to conductivity from superconducting fluctuations (SF) at $T > T_c$ and weak localization^{25–30} (see SI for details), we fit the experimental data (dashed green lines in Fig. 1). These SF-fits, in which critical temperature T_c enters as the adjustable parameter, yield the macroscopic value of T_c . For all samples, the extracted T_c (given in Table) is very close to the temperature of the inflection point, i.e. the temperature where dR/dT is maximal³¹, and lies at the foot of $R_{\square}(T)$ ³². All Sets demonstrate the suppression of T_c with the increase of sample's ‘normal’ sheet resistance (insets in Fig. 1). In fermionic scenario, the suppression of T_c follows celebrated Finkelstein’s formula³:

$$\ln\left(\frac{T_c}{T_{c0}}\right) = \frac{1}{|\gamma|} - \frac{1}{\sqrt{2r}} \ln\left(\frac{\gamma - r/4 - \sqrt{r/2}}{\gamma - r/4 + \sqrt{r/2}}\right), \quad (1)$$

where $\gamma = 1/\ln(kT_{c0}\tau/\hbar)$ (T_{c0} is superconducting critical temperature of a clean sample) and $r = G_{00}R_{\square N}$, where the choice of ‘normal state’ sheet resistance is uncertain due to strong non-monotonic $R_{\square}(T)$ dependence. Usually, to analyze the suppression of T_c with disorder, T_c is plotted vs. resistance at some temperature^{33,34}. For our samples we plot T_c vs. R_{\max} , the resistance in the maximum prior to superconducting resistance drop.

The BKT transition manifest itself both in the power-law behaviour of current-voltage characteristics $V \propto I^{\alpha \geq 3}$ and in exponential decay of resistance:

$$R(T) \propto \exp(T/T_{\text{BKT}} - 1)^{-1/2}. \quad (2)$$

The first method for finding T_{BKT} is to utilize power-law fits to the I - V characteristics for which the switch from $V \propto I$ to $V \propto I^3$ occurs at the transition (Fig. 2 (a)). The second method is to replote $R(T)$ (see Eq. (2)) as $d(\ln R/dT)^{-2/3}(T)$ ³⁵. If the decay of resistance is due to vortex motion the experimental curve is linear in these coordinates and the intersection of experimental curve with axis X corresponds to T_{BKT} (Fig. 2 (c), (d) and Fig. 5 in SI). As was demonstrated for ALD deposited TiN films³⁰, these methods provide BKT temperatures that coincide within one percent. Below we utilize both methods to observe BKT transition or it’s absence in a system.

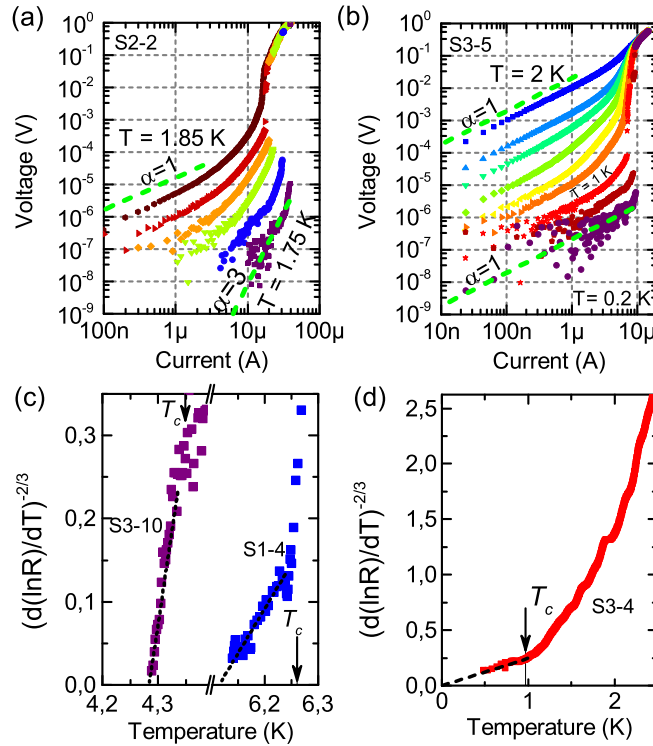


Figure 2. (a), (b) Temperature evolution of current-voltage characteristics on a log-log scale for samples S2-2 and S3-5. Dashed line indicate the slopes corresponding to power $\alpha = 1$ and $\alpha = 3$ on the $V \propto I^{\alpha}$. (c), (d) Rescaling of the sheet resistance $R_{\square}(T)$ to the BKT form to extract the vortex-unbinding temperature T_{BKT} (Eq. (2)) for samples S1-4, S3-10 (c) and sample S3-4 (d), where the straight line (dashed) corresponds to Eq. (2). Arrows mark position of T_c . Notably, the $R_{\square}(T)$ curves obey Eq. (2) just at $T < T_c$. The value $(d(\ln R)/dT)^{-2/3} = 0$ at T_{BKT} .

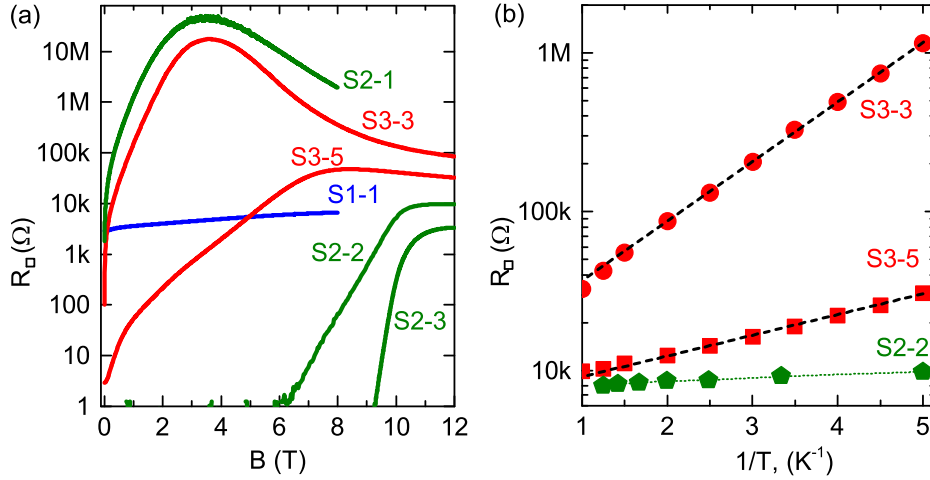


Figure 3. (a) Magnetoresistance per square $R_{\square}(B)$ on semi-log scale for films listed in figure. All curves are taken at temperature $T = 0.2$ K, except for $R_{\square}(B)$ of sample S1-1 that is obtained at $T = 0.04$ K. (b) Arrhenius plot of sheet resistance R_{\square} in constant perpendicular magnetic field vs. $1/T$ on for samples S3-3 ($B=1.7$ T), S3-5 ($B=6.8$ T) and S2-2 ($B = 11.3$ T). Dashed lines show the activation dependence $R = R_1 \exp(E_1/k_B T)$, where for S3-3 $R_1=5.3$ k Ω , $E_1=86$ meV and for S3-5 $R_1=2.3$ k Ω , $E_1=26$ meV. Sample S2-2 exhibits saturation (not activation).

Suppression of superconductivity in Set-1

Figure 1 (a) demonstrates that the SF-fitting describes fairly well the gradual decrease in the resistance $R_{\square}(T)$ matching perfectly the experimental points down to values $\approx 0.2 \cdot R_{\max}$ (without any additional assumptions about mesoscopic inhomogeneities³⁶). Below T_c the $R_{\square}(T)$ follows Eq. (2) (see Fig. 2 (c) and Fig. 5 in SI) and, hence, is caused by motion of free vortices. The obtained T_{BKT} temperatures are listed in Table.

The values of T_c plotted vs. R_{\max} (inset of Fig. 1 (a)) show that the suppression of T_c is in accord with Eq. (1), with fitting parameter $\gamma=6.5$. The macroscopic superconductivity in samples is fully suppressed before sample's R_{\max} reaches R_q . Figure 3 (a) shows $R_{\square}(B)$ curve of non-superconducting sample S1-1 taken at $T = 0.04$ K. The resistance depends weakly on magnetic field (without a magnetoresistance peak presented in samples with close R_{\max} value from other Sets), implying the lack of Cooper pairs in the sample.

To sum up, the Set-1 exhibits the superconductor-metal transition in agreement with fermionic scenario.

Suppression of superconductivity in Set-2

Figure 1 (b) shows that the gradual resistance drop of $R_{\square}(T)$ is in agreement with the SF-fitting. We observe that both the power-law $V(I)$ curves (Fig. 2(a)) and $R(T)$ dependencies at $T < T_c$ (see Fig. 5 in SI) are in agreement with standard BKT theory without any additional assumptions about effect of disorder³⁶ even for sample S2-2 that has $R_{\max} \lesssim R_q$.

The suppression of T_c in Set-2 (inset in Fig. 1 (b)) is described with the fitting parameter $\gamma=4.4$. That is slightly below the applicability limit of Eq. (1) which is $\gamma \simeq 5$. Unfortunately, we do not have samples between S2-1 and S2-2 so we can not tell, how T_c gets suppressed in region $R_{\max} > R_q$. The sample S2-1 experiences substantial resistance drop, but the global coherent superconducting state is not achieved at lowest temperatures. The behavior of $R_{\square}(T)$ suggests that the film falls into the Bose metallic state, featuring a finite density of free vortices.

Magnetic field reveals huge difference between $R_{\square}(B)$ of sample S2-1 ($R_{\max} > R_q$) and samples S2-2, S2-3 ($R_{\max} < R_q$) (Fig. 3 (a)). The magnetoresistance of S2-1 shoots up with slight increase of magnetic field from zero, unlike samples with $R_{\max} < R_q$ where resistance appears in strong magnetic field and increases relatively slow. Then $R_{\square}(B)$ for S2-1 reaches a maximum, followed by decrease of $R_{\square}(B)$. We do not see maximum for S2-2 and S2-3 since for superconducting samples it appears at higher fields¹². As was shown in details in²³, in constant magnetic field sample S2-1 demonstrates the temperature-driven charge BKT transition into superinsulating state^{23,37} — the state also found in the InO films^{38,39}.

To sum up, the behaviour of Set-2 suggests the action of both fermionic and bosonic mechanisms of supercon-

ductivity suppression.

Suppression of superconductivity in Set-3

The films of Set-3 fall into two categories depending on the ratio between R_{\max} and R_q (Fig. 1 (c)). For films with $R_{\max} < R_q$ the $R_{\square}(T)$ decrease with cooling down is in agreement with the conventional theories of superconducting fluctuations and Berezinskii-Kosterlitz-Thouless transition (Fig. 2 (c)), where both T_{BKT} and T_c decrease with R_{\max} increasing (see Table). The films with $R_{\max} > R_q$ show the significant resistance drop (from few orders of magnitude for sample S3-5 to one order for S3-1) the substantial part of which is in agreement with the SF-fits, implying there are short living Cooper pairs in a system. After deviating from the SF-fits, the $R_{\square}(T)$ either saturates (samples from S3-5 to S3-2) like a Bose metal or increases exponentially (S3-1, S3-0) like an insulator (thinner films, not shown in Fig. 1 (c), are insulators⁴²).

The T_c obtained from the SF-fits decreases with R_{\max} increasing (inset in Fig. 1 (c)). Equation (1) describes the T_c suppression but only for samples with $R_{\max} < R_q$ and with quite small $\gamma=3.8$, when normally $\gamma \gtrsim 5$ in fermionic model. For samples with $R_{\max} > R_q$ the critical temperature T_c decreases slower than Eq. (1) predicts.

Films with $R_{\max} > R_q$ do not experience the BKT transition. Particularly, for S3-5 and S3-4 the $R(T)$ demonstrates decay in accord with Eq. (2) but yields $T_{\text{BKT}} = 0$ (Fig. 2(d)) and $V(I)$ curves in low-current limit remain linear $V \propto I^{\alpha=1}$ at all measured temperatures (Fig. 2 (b)). This could be due to inhomogeneities of samples, but the estimation of inhomogeneity scale L ⁴⁰ provides the values $L \simeq 3 - 6 \mu\text{m}$. This is few orders of magnitude larger than inhomogeneities observed from electronic and atomic-force microscopy. Even though the exponent α remain $\alpha = 1$, the voltage jumps to normal resistance branch with increasing I appear at low temperatures. In disordered ALD deposited TiN films, these voltage jumps in $V(I)$ occur at $T \simeq T_{\text{BKT}}$, i.e. when α switches from 1 to 3⁴¹. Hence, we observe that the T_{BKT} transition vanishes while T_c remains non-zero.

Representative magnetoresistance curves of samples with $R_{\max}(B=0) > R_q$ (S3-3 and S3-5) are given in Fig. 3(a). Both observed features - the magnetoresistance (MR) peak and fast increase of $R_{\square}(B)$ in weak magnetic field - become more pronounced with sample's $R_{\max}(B=0)$ increasing. Finally, the behaviour of $R_{\square}(T, B = \text{const})$ in constant magnetic field (which is slightly smaller than field where $R_{\square}(B) = \text{max}$) is given in Fig. 3(b). Samples with $R_{\max}(B=0) > R_q$ demonstrate typical insulating dependence $R = R_I \exp(E_I/k_B T)$. The giant MR peak and Arrhenius behavior of the resistance near it may be found in systems in which there are large fluctuations in the amplitude of the superconducting order parameter². Experimentally these fluctuations appear to be helped by compositional variations on a mesoscopic scale². Apparently, the mesoscopic compositional variations emerge in our Sets with decreasing deposition temperature T_{ALD} and increasing fraction of Ti x .

To sum up here, for superconducting films with $R_{\max} > R_q$, the T_{BKT} transition vanishes while T_c remains non-zero. This is typical for bosonic scenario of suppression of superconductivity^{4,5}. Bearing in mind that T_c gets suppressed with disorder we conclude that for Set-3 both bosonic and fermionic mechanisms suppress superconductivity.

Conclusion

We have examined three sets of superconducting disordered thin $\text{Nb}_{1-x}\text{Ti}_x\text{N}$ films, where the only difference between sets was the fraction of Ti x and/or the temperature of deposition T_{ALD} . We showed that, both increase of x and the decrease of T_{ALD} , lead to the smooth crossover from fermionic mechanism of superconductivity suppression to the case where both bosonic and fermionic mechanisms are involved. We show that the ratio between R_{\max} , and $R_q = h/4e^2$ divides films of all sets into two categories. For moderately disordered films ($R_{\max} < R_q$) the superconducting transition is in agreement with the conventional theories of superconducting fluctuations and Berezinskii-Kosterlitz-Thouless transition, and T_c decreases with disorder in accord with the Finkel'stein formula. For critically disordered films ($R_{\max} > R_q$) the T_c decreases slower than the Finkel'stein formula predicts. Moreover, films with $R_{\max} > R_q$ do not experience the BKT transition to zero-resistance state. Careful magnetoresistance measurements revealed that there is a qualitative difference between films with R_{\max} smaller and greater than R_q .

Methods

The fabrication is built upon the Atomic Layer Deposition technique. The structure of films grown on Si substrates with AlN buffer layers was investigated using a JEOL-4000EX electron microscope operated at 400 kV, with a point-to-point resolution of 0.16nm and a line resolution of 0.1 nm.

Measurement technique

The films were lithographically patterned into bridges 50 μm wide, the distance between current-contacts was 2500 μm and distance between voltage-contacts was 450 μm . Low resistive transport measurements ($R(B, T) < 1\text{M}\Omega$) are carried out using low-frequency ac and dc techniques in a four-probe configuration $I = 1 - 10\text{ nA}$, $f \approx 3\text{ Hz}$. High resistive transport measurements ($R(B, T) > 1\text{M}\Omega$) are carried out using low-frequency ac and dc techniques in a two-probe configuration with $V \approx 100\ \mu\text{V}$, $f \approx 1\text{ Hz}$. For ac measurements we use one/two SR830 Lock-ins and current/voltage preamplifiers SR570/SR560. For dc measurements we use sub-femtoampermeter Keythley 6430a and nanovoltmeter Agilent 34420. All resistance measurement are carried out in linear regime with using adequately system of filtration. Resistivity measurements at sub-Kelvin temperatures were performed in dilution refrigerators $^3\text{He}/^4\text{He}$ with superconducting magnet.

Table

Table 1. T_{ALD} is the deposition temperature; d is film thickness; R_{max} is the resistance at the maximum of $R(T)$; R_{77} is the resistance per square at $T = 77\text{ K}$; T_c is the critical temperature determined from the SF-fits; T_{BKT} is BKT transition temperature; D is the diffusion coefficient $D = 0.882 \cdot T_c / (eB_{c2})$ (see Fig. 2 in SI for B_{c2}); n is the Hall carrier density (see SI).

sample $\text{Nb}_{1-x}\text{Ti}_x\text{N}$		d (nm)	R_{max} (k Ω)	R_{77} (k Ω)	T_c (K)	T_{BKT} (K)	D $\frac{\text{cm}^2}{\text{s}}$	n $\frac{10^{22}}{\text{cm}^3}$
$T_{\text{ALD}}=450^\circ\text{C}$	Set-1, $x = 0.3$ S1-1	3	3.96	2.56	0	0		
	S1-2	10	0.75	0.69	4.85	4.79		
	S1-4	20	0.18	0.17	6.26	6.11		
$T_{\text{ALD}}=350^\circ\text{C}$	Set-2, $x=0.3$ S2-1	10	17.55	4.52	0	0	0.2	0.5
	S2-3	15	2.66	1.69	3.27	3.08		
	S2-5	40	0.52	0.77	4.33	4.18		
$T_{\text{ALD}}=350^\circ\text{C}$	Set-3, $x = 0.33$ S3-1	9.2	17.9	—	—	0	0.3	1
	S3-2	9.2	15.72	—	—	0		
	S3-3	9.2	15.18	5.75	0.75	0		
	S3-4	9.2	14.13	—	0.97	0		
	S3-5	10	9.26	4.53	1.7	0		
	S3-7	12	2.24	1.87	3.85	3.81		
	S3-9	19	1.87	0.98	4.28	4.26		
S3-10	21	0.8	0.69	4.35	4.29			

References

1. Gantmakher, V. F. & Dolgoplov, V. T. Superconductor-insulator quantum phase transition. *Physics-Uspeski* **53**, 3 (2010).
2. Lin, Y-H., Nelson, J. & Goldman, A.M. Superconductivity of very thin films: the superconductor-insulator transition. *Physica C* **514**, 130 (2015).
3. Finkel'stein, A. M. Suppression of superconductivity in homogeneously disordered systems. *Physica B* **197**, 636 (1994).
4. Gold, A. Dielectric properties of a disordered Bose condensate. *Physical Review A* **33**, 652 (1986).
5. Fisher, M. P. A., Grinstein, G. & Grivin, S. Presence of quantum diffusion in two dimensions: Universal resistance at the superconductor-insulator transition. *Physical Review Letters* **64**, 587 (1990).
6. Yong, J., Lemberger, T. R., Benfatto, L., Ilin, K. & Siegel, M. Robustness of the Berezinskii-Kosterlitz-Thouless transition in ultrathin NbN films near the superconductor-insulator transition. *Physical Review B* **87**, 184505 (2013).

7. Makise, K. *et al.* Superconductor-insulator transition in two-dimensional NbN/MgO and NbN/AlN/MgO films. *Materials Research Express* **2**, 106001 (2015).
8. Hebard, A. F. & Paalanen, M. A. Magnetic-field-tuned superconductor-insulator transition in two-dimensional films. *Physical Review Letters* **65**, 927 (1990).
9. Shahar, D., Ovadyahu, Z. & Goldman, A. M. Superconductivity near the mobility edge, *Physical Review B* **46**, 10917 (1992).
10. Gantmakher, V. F. *et al.* Superconductor-insulator transition in amorphous In-O films. *Physica B* **284**, 649 (2000).
11. Hadacek, N., Sanquer, M. and Villegier, J.-C. Double reentrant superconductor-insulator transition in thin TiN films. *Physical Review B* **69** 024505 (2004).
12. Baturina, T. I., Mironov, A. Yu., Vinokur, V. M., Baklanov, M. R. & Strunk, C. Localized superconductivity in the quantum-critical region of the disorder-driven superconductor-insulator transition in TiN thin films. *Phys. Rev. Lett.* **99**, 257003 (2007).
13. Das, D. & Doniach, S. Existence of a Bose metal at $T = 0$. *Phys. Rev. B* **60**, 1261 (1999).
14. Phillips, P. & Dalidovich, D. The Elusive Bose Metal, *Science* **302**, 243 (2003).
15. Diamantini, M. C., Trugenberger, C. A., Lukyanchuk, I. & Vinokur, V. M. Gauge Topological Nature of the Superconductor-Insulator Transition. Preprint at <https://arxiv.org/abs/1710.10575>
16. Burmistrov, I. S., Gornyi, V. & Mirlin, A. D. Superconductor-insulator transitions: Phase diagram and magnetoresistance. *Physical Review B* **92**, 014506 (2015).
17. Tamir, I. *et al.* Sensitivity of the superconducting state in thin films. *Science Advances* **5**, eaau3826 (2019).
18. Lim, B. S., Rahtu, A. & Gordon, R. G. Atomic layer deposition of transition metals. *Nature Materials* **2**, 749 (2003).
19. Driessen, E. F. C., Coumou, P. C. J. J., Tromp, R. R., de Visser, P. J. & Klapwijk, T. M. Strongly disordered TiN and NbTiN s-wave superconductors probed by microwave electrodynamics. *Phys. Rev. Lett.* **109**, 107003 (2012).
20. Makise, K., Terai, H., Tominari, Y., Tanaka, S. & Shinozaki, B. Duality picture of superconductor-insulator transitions on superconducting nanowire. *Sci. Rep.* **6**, 27001 (2016).
21. Proslir, T., Klug, J. A., Becker, N. C., Elam, J. W. & Pellin, M. J. Atomic layer deposition of superconductors. *ECS Transactions* **41**, 237 (2011).
22. Shiino, T. *et al.* Improvement of the critical temperature of superconducting NbTiN and NbN thin films using the AlN buffer layer. *Supercond. Sci. Technol.* **23**, 045004 (2010).
23. Mironov, A. Yu. *et al.* Charge Berezinskii-Kosterlitz-Thouless transition in superconducting NbTiN films. *Scientific Reports* **8**, 4082 (2018).
24. Hazra, D. *et al.* Superconducting properties of NbTiN thin films deposited by high-temperature chemical vapor deposition *Physical Review B* **97**, 144518 (2018).
25. Aslamasov, L. G. & Larkin, A. I. The influence of fluctuation pairing of electrons on the conductivity of normal metal, *Physics Letters A* **26**, 238 (1968).
26. Maki, K. The critical fluctuation of the order parameter in type-II superconductors, *Progress of Theoretical Physics* **39**, 897 (1968).
27. Thompson, R. S. Microwave, flux flow and fluctuation resistance of dirty type-II superconductors, *Physical Review B* **39**, 327 (1970).
28. Altshuler, B. L., Aronov, A. G. & Lee, P. A. Interaction Effects in Disordered Fermi Systems in Two Dimensions, *Physical Review Letters* **44**, 1288 (1980).
29. Lopes dos Santos, J. M. B., Abrahams, E. Superconducting fluctuation conductivity in a magnetic field in two dimensions, *Physical Review B* **31**, 172 (1985).
30. Postolova, S. V., Mironov, A. Yu. & Baturina, T. I. Nonequilibrium transport near the superconducting transition in TiN films, *JETP Letters* **100**, 635 (2015).

31. Baity, P. G., Shi, X., Shi, Z., Benfatto, L. & Popovic, D. Effective two-dimensional thickness for the Berezinskii-Kosterlitz-Thouless-like transition in a highly underdoped $\text{La}_{2-x}\text{Sr}_x\text{CuO}_4$. *Physical Review B* **93**, 024519 (2016).
32. Baturina, T. I. *et al.* Superconducting phase transitions in ultrathin TiN films. *Europhys. Lett.* **97**, 17012 (2012).
33. Noat, Y., *et al.* Unconventional superconductivity in ultrathin superconducting NbN films studied by scanning tunneling spectroscopy. *Physical Review B* **88**, 014503 (2013).
34. Postolova, S. V., Mironov, A. Yu., Baklanov, M. R., Vinokur, V. M. & Baturina, T. I. Reentrant Resistive Behavior and Dimensional Crossover in Disordered Superconducting TiN Films *Scientific Reports* **7**, 1718 (2017).
35. Kessler, B. M., Girit, Ç, Ö., Zettl, A. & Bouchiat, V. Tunable Superconducting Phase Transition in Metal-Decorated Graphene Sheets *Physical Review Letters* **104**, 047001 (2010).
36. König, E. J., *et al.* Berezinskii-Kosterlitz-Thouless transition in homogeneously disordered superconducting films *Physical Review B* **92**, 214503 (2015).
37. Vinokur, V. M. *et al.* Superinsulator and quantum synchronization. *Nature* **452**, 613 (2008).
38. Ovadia, M. *et al.* Evidence for a Finite-Temperature Insulator. *Scientific Reports* **5**, 13503 (2018).
39. Tamir, I. *et al.* Excessive noise as a test for many-body localization. *Physical Review Letters* **99**, 035135 (2019).
40. Benfatto, L., Castellani, C., & Giamarchi, T. Broadening of the Berezinskii-Kosterlitz-Thouless superconducting transition by inhomogeneity and finite-size effects. *Physical Review B* **80**, 214506 (2009).
41. Qiao, L., Li, D., Postolova, S. V., Mironov, A. Yu., Vinokur, V. & Rosenstein B. Dynamical instability of the electric transport in superconductors. *Scientific Reports* **8**, 14104 (2018).
42. Burdastyh, M. V. *et al.* Superconductor-Insulator Transition in NbTiN Films. *JETP Letters* **106**, 749 (2017).
43. Ephron, D. *et al.* Observation of Quantum dissipation in the vortex state of a highly disordered superconducting thin film. *Physical Review Letters* **76**, 1529 (1996).
44. Christiansen, C., Hernandez, L. M., Goldman A. M. Evidence of collective charge behavior in the insulating state of ultrathin films of superconducting metals. *Physical Review Letters* **88**, 037004 (2002).
45. Leng, X. *et al.* Electrostatic control of the evolution from a superconducting phase to an insulating phase in ultrathin $\text{YBa}_2\text{Cu}_3\text{O}_{7-x}$ films. *Physical Review Letters* **107**, 027001 (2011).
46. Tsen, A. W., *et al.* Nature of the quantum metal in a two-dimensional crystalline superconductor. *Nature Physics* **12**, 208 (2016).
47. Breznay, N. P., Kapitulnik, A. Particle-hole symmetry reveals failed superconductivity in the metallic phase of two-dimensional superconducting films, *Science Advances* **3**, e1700612 (2017).

Acknowledgements

The experimental work was supported by grant of RF president (MK-5455.2018.2). The work at Argonne (V.M.V. and T.P.) was supported by the U.S. Department of Energy, Office of Science, Basic Energy Sciences, Materials Sciences and Engineering Division. The Hall and magnetoresistance measurements of sample S3-9 performed in IPM PAS was supported by RSF, project No. 15-12-10020. We are grateful to Dr. Tatyana I. Baturina for initiating the work on NbTiN films.

Author contributions statement

The films were synthesized by TP; AYuM, SVP, MVB carried out the experiments; SVP, SSU, AVA carried out magnetoresistance measurements of sample S3-9; AYuM, SVP and VMV analyzed the data. All authors discussed the results and contributed in writing the manuscript.

Additional information

The authors declare that they have no competing interests as defined by Nature Research, or other interests that might be perceived to influence the results and/or discussion reported in this paper.

Data availability

The authors declare that all relevant data supporting the findings of this study are available within the article and its supplementary information file. Additional raw data, if necessary, are available upon request to AYuM, mironov@isp.nsc.ru